ELSEVIER

Solar Energy Materials & Solar Cells 74 (2002) 183–193

Solar Energy Materials & Solar Cells

www.elsevier.com/locate/solmat

Spatial distribution of minority-carrier lifetime and local concentration of impurities in multicrystalline silicon solar cells

Ken-ichi Kurobe*, Mineo Miura, Kenji Hirano, Hiroyuki Matsunami

Department of Electronic Science and Engineering, Kyoto University, Yoshida-Honmachi, Sakyo, Kyoto 606–8501, Japan

Abstract

Spatial distribution of minority-carrier lifetime (τ) in multicrystalline silicon solar cells was investigated. By mapping of τ, a wide distribution in a higher-efficiency cell and a narrow distribution in a lower-efficiency cell was found, respectively. Based on the relation between τ and the density of grain boundaries, spatial distribution of impurities was characterized by secondary ion mass spectrometry. To clarify the spatial profile near grain boundaries, a method of changing detection area was carried out. Iron (Fe) segregation within 100 μm around a grain boundary was observed. In the lower-efficiency cell, a measurable amount of Fe was contained in a crystalline area as well.

Keywords: Multicrystalline silicon; Solar cell; Lifetime; Distribution; Grain boundary; SIMS; Iron; Segregation

1. Introduction

Multicrystalline silicon (Mx-Si) solar cells are produced in a large scale because they have a reasonable conversion efficiency (η) and their fabrication processes are adequate for mass production. A conversion efficiency of more than 17% has been obtained on 15 cm × 15 cm Mx-Si solar cells [1] and of 19.8% has been achieved using a laboratory-scaled process [2]. Mx-Si solar cells, however, have in fact various efficiencies or dispersion on crystallinity in each cell by unintentionally doped

*Corresponding author.
E-mail address: k-kurobe@kuee.kyoto-u.ac.jp (K.-i. Kurobe).

0927-0248/02/$ - see front matter
PII: S0927-0248(02)00063-6

impurities or many grain boundaries, which are brought during wafer-fabrication processes.

There are many parameters to indicate solar cell performance. Short-circuit current density (J_{sc}), especially, is an important one for Mx-Si solar cells. Grain boundaries and some impurities in wafers affect minority-carrier lifetime (τ) and correlate with J_{sc}. It is an important matter to investigate the correlation between the distribution of τ and the performance of Mx-Si solar cells.

The authors have investigated macroscopic distribution of τ in Mx-Si solar cells which have various efficiencies, and discussed the effects of grain boundaries on τ. Next, secondary ion mass spectrometry (SIMS) with changing ion-detection areas is proposed. The spatial distribution of impurity concentration around grain-boundary areas and crystalline areas was characterized.

2. Experimental

For measurement of τ in cast Mx-Si solar cells, three cells with different efficiencies named cells—A, B, and C, were selected, the photovoltaic characteristics of which are given in Table 1. Fig. 1 shows an experimental procedure to characterize solar cells in this paper. The solar cells of 12.5 cm^2 were divided into 10×10 ($= 100$) samples using a diamond cutter. The size of each sample has 12 mm $\times$ 12 mm of area and 300 μm of thickness. Those cells have a conventional $n^+/p/p^+$ structure and silicon nitride passivation coating. The junction depth of the cell was about 0.2–0.3 μm. Four silver finger electrodes were aligned with intervals of 3 mm on each sample, and some samples have a bus bar which is perpendicular to the finger electrodes.

To determine minority-carrier lifetime in n^+–p solar cells, reverse recovery switching transient analysis was used. Edges of a sample hardly affect τ as mentioned below. The electron diffusion length (L_e) is given by

$$L_e = \sqrt{D\tau}, \tag{1}$$

where D is the diffusion constant and is estimated as about 30 cm^2/s for a carrier density of 1×10^{16} cm^{-3} at room temperature. L_e is calculated to be at most 400 μm for a τ of 50 μs, which is smaller than the side length of those samples (12 mm). Thus, the edges of the samples affect little the measured value of τ.

Table 1
Photovoltaic characteristics of cells-A, -B, and -C (100 mW/cm^2, AM1.5)

	V_{oc} (V)	J_{sc} (mA/cm^2)	FF	η (%)
Cell-A	0.602	32.7	0.732	14.4
Cell-B	0.576	30.9	0.712	12.6
Cell-C	0.567	28.3	0.689	11.0

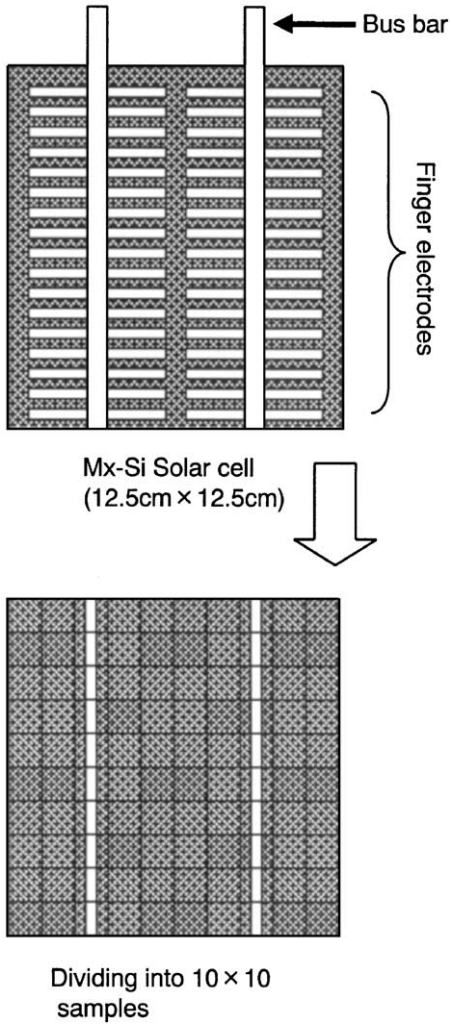

Fig. 1. Experimental procedure to characterize solar cells. The upper drawing indicates a schematic view of a solar cell before dividing. Three solar cells (cells-A, -B, and -C) with different efficiencies were divided into 10×10 samples, shown in lower drawing. Each sample has a size of 12 mm $\times$ 12 mm.

The transient behavior of n^+–p diodes is described [3] as

$$\operatorname{erf}\sqrt{\frac{t_s}{\tau}} = \frac{1}{1 + I_r/I_f}, \tag{2}$$

where t_s, I_f and I_r mean the storage time, forward and reverse current, respectively.

For the switching transient analysis, square-wave pulse voltage with a duty ratio of 50% was applied and a current form was measured with a digital oscilloscope. The forward and reverse voltages were set as +2 V and −2 V, respectively. The τ of

each sample was measured by using one of the finger electrodes located at the center of a sample.

3. Results and discussion

3.1. Macroscopic distribution of lifetime in solar cells

Fig. 2 shows contour maps of τ in each cell. Fig. 2(s) shows a layout of 10×10 ($= 100$) samples. In Figs. 2(a)–(c), gradation at each grid point corresponds to the measured τ of each sample. In cell-A, many samples give more than 30 μs of τ except the lower edge and near bus bars. In cell-B, the number of samples with

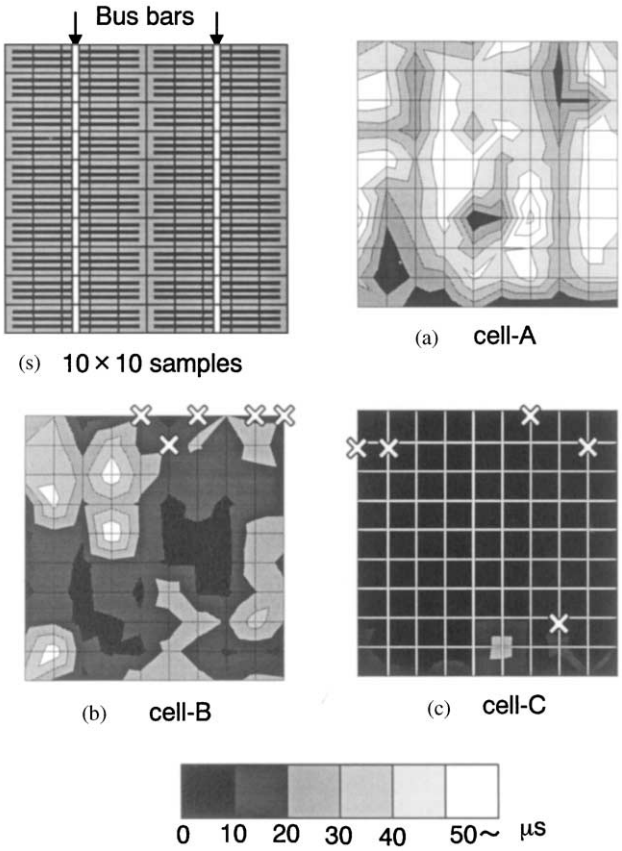

Fig. 2. Contour maps of τ in each cell. The lifetime τ was measured at the center part of each sample for 10×10 samples in (s). The measured τ was drawn at a corresponding grid point in (a)–(c). "×" marks mean samples which could not be measured due to bad electrical connection.

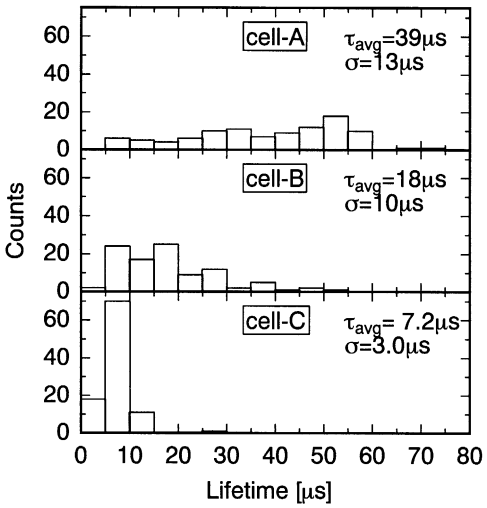

Fig. 3. Histograms of τ in each cell. Each frequency distribution was taken from reverse recovery switching measurement on 10×10 samples.

10–20 μs of τ increases. In cell-C, samples with less than 10 μs of τ occupied the cell. The average value of τ for each cell corresponds to J_{sc} given in Table 1.

Fig. 3 shows the histograms of τ in each cell. In cell-A, the average of τ in all samples is 39 μs. Wide distribution of τ is found.

In cells-B and -C, the averages are 18 and 7.2 μs, respectively. The distribution of τ in cell-B is similar to that in cell-A, while it is narrow in cell-C. The standard deviations (σ) of τ in cells-A, B, and C are 13, 10, and 3.0 μs, respectively.

3.2. *Effects of grain boundaries on the lifetime*

In order to investigate the effects of grain boundaries on τ, detailed measurement of τ was carried out for a sample without a bus bar. The sample was divided into 4×4 ($= 16$) square mesas with a side length of 3 mm using a diamond cutter. A passivation-coating layer and all finger electrodes of each mesa were not removed.

To characterize the effects of grain boundaries, the density of grain boundaries was defined as the total length of grain boundaries per unit area, observed by a Nomarski Microscope. Stacking faults, which have a feature of many line shapes, were not counted for the measurement.

The electron diffusion length was estimated as at most 400 μm as described previously. The side length of each square mesa is about 3 mm, and thus minority-carrier recombination on the side wall of each mesa hardly affects the measured τ.

Fig. 4 shows the correlation between the density of grain boundaries and τ. The measured τs range from 15 to 35 μs in cell-A, and almost all mesas have a trend of decrease in τ with increasing the density of grain boundaries. In cell-C, on the

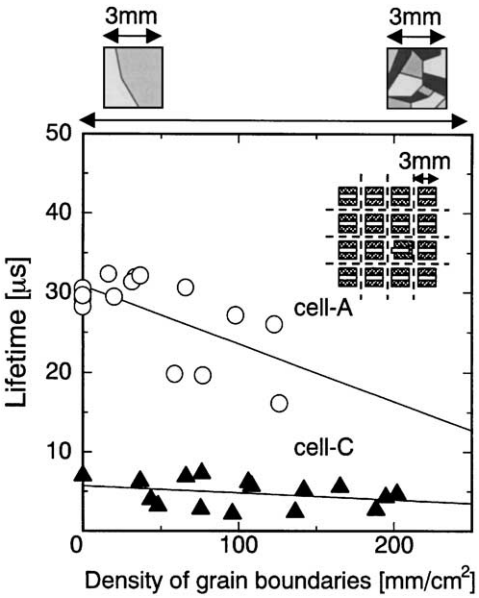

Fig. 4. Correlation between density of grain boundaries and lifetime. Strong correlation is observed for cell-A and weak correlation for cell-C.

contrary, the measured τs were constant irrespective of the density of grain boundaries. This result suggests the difference of impurity distribution for cells-A and -C.

3.3. Depth profile of impurities with SIMS analysis

In order to investigate the effects of grain boundaries, a spatial profile of impurities in cell-A was measured with SIMS analysis using cesium (Cs) and oxygen (O) ions. All electrodes and passivation coating were removed from the surface of a sample with hydrochloric and phosphoric acid. At first, an analysis on impurity depth profiles was carried out. The side length of a raster area, in which the surface is equally and constantly sputtered by ions, was 300 μm. The side length of detection area (L_D), where the number of detected secondary ions was counted, was 60 μm.

Fig. 5 shows the depth profile of impurities in a grain boundary area and a crystalline area. Phosphorus (P), as a dopant of n^+ layer and iron (Fe), as a typical lifetime killer in silicon [4], were detected. As to P, the same profiles were obtained in the both grain boundary and crystalline areas. Fe has a flat profile, and the concentration of Fe in the grain boundary area is about 10 times larger than that in the crystalline area.

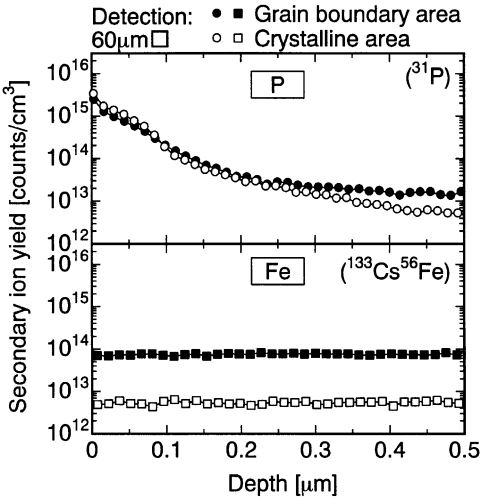

Fig. 5. Depth profile of impurities in grain boundary area and crystalline area.

3.4. Spatial profile of Fe impurities with SIMS analysis

In order to examine the spatial distribution of impurities near grain boundaries minutely, a new procedure in SIMS analysis is proposed. The procedure of detecting impurity distribution near grain boundaries by SIMS analysis is as follows:

(1) Aligning the center of a raster area with a grain boundary.
(2) Measuring secondary ion-signal counts in a detection area per unit depth (20 nm). The detection area was changed from 300 to 20 μm counts.
(3) Plotting secondary ion yield for variable detection areas.

Fig. 6 shows a schematic for SIMS analysis with variable detection areas. Given that the impurity concentration is constant along the sputtering direction and is axisymmetric around the grain boundary, the measured secondary ion concentration $C_{\mathrm{ion}}(L_{\mathrm{D}})$, which is proportional to the secondary ion yield, is expressed by

$$C_{\mathrm{ion}}(L_{\mathrm{D}}) = \frac{1}{L_{\mathrm{D}}} \int_{-L_{\mathrm{D}}/2}^{L_{\mathrm{D}}/2} C(x)\,\mathrm{d}x, \tag{3}$$

where $C(x)$ indicates the impurity concentration.

If impurities are uniformly distributed in the grain boundary area, W_{G}, $C(x)$ is expressed by $C(x) = C_{\mathrm{G}}$ for $|x| \leqslant W_{\mathrm{G}}/2$ and C_{C} for $|x| > W_{\mathrm{G}}/2$, where C_{G} is the maximum impurity concentration at the center of a grain boundary ($x = 0$), and C_{C} is the background concentration at the crystalline area.

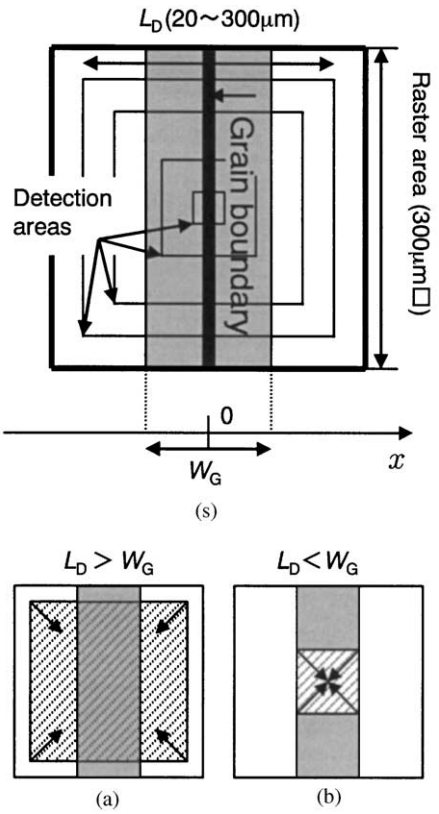

Fig. 6. Schematic for SIMS analysis with variable detection area (s). Surface is equally and constantly sputtered in raster area, and mass detection was carried out in detection area. (a) For $L_D > W_G$, average concentration is low and changed. (b) For $L_D < W_G$, average concentration is high and constant.

The secondary ion yield is expressed as

$$C_{ion}(L_D) = \begin{cases} C_G, & (0 \leqslant L_D \leqslant W_G), \\ C_C + (C_G - C_C)W_G/L_D, & (W_G < L_D), \end{cases} \tag{4}$$

as shown in Fig. 7(a).

If impurities are exponentially distributed, with $W_G \to 0$, $C(x)$ is expressed by $C(x) = C_G \exp(-|x|)$, and then,

$$C_{ion}(L_D) = \frac{2C_G}{L_D}\{1 - \exp(-L_D/2)\}, \tag{5}$$

as shown in Fig. 7(b).

Fig. 8 shows the measured secondary ion concentration of Fe versus the side length in detection areas. In the range with a L_D of more than 100 μm, the concentration is inversely proportional. In the range with a L_D of less than 100 μm,

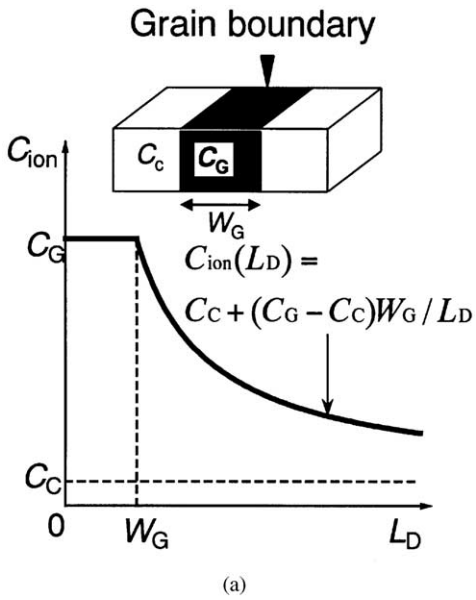

Fig. 7. Schematic of real-space profile for impurities and theoretical curves which are shown as secondary ion concentration versus side length of detection area. (a) Uniform distribution, (b) exponential distribution.

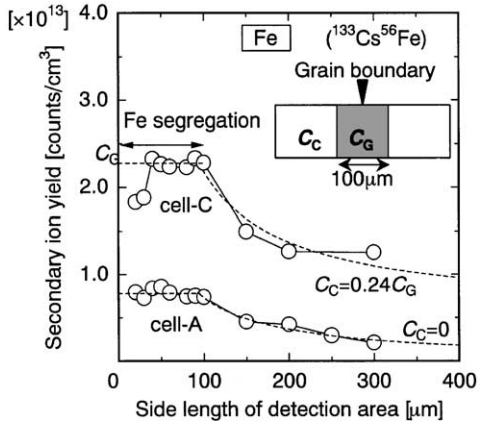

Fig. 8. Measured secondary ion yield of Fe versus side length of detection area. Impurity profile near grain boundary is similar to Fig. 7(a). In cell-A, impurity decreases with increasing side length of detection area, whereas in cell-C it shows saturation tendency ($C_C = 0.24C_G$).

on the other hand, the concentration is almost fixed. This result means that the impurities are segregated into a grain-boundary area within 100 μm. This profile of concentration is similar to Fig. 7(a).

In cell-C, a measurable amount of Fe ($\approx 0.24C_G$) is contained in spite of outside the grain boundary area. From this result, the difference of τ-distribution can be explained. In cell-A, only grain boundaries affect the measured τ. The grain boundaries are randomly allocated, and therefore τ-distribution becomes wide. In cell-C, τ in crystalline areas is small, which affects the measured τ. τ-distribution is narrow because the effects of grain boundaries become very small.

4. Conclusions

Spatial distribution of τ in Mx-Si solar cells was investigated. By mapping and a histogram analysis of τ, a distinct difference of τ-distribution was found. The cell with higher efficiency has a larger average and wider σ of τ than the cell with lower efficiency. Based on the result that the density of grain boundaries affects τ, a SIMS analysis was carried out. In the spatial profile of impurities, Fe segregation in the 100 μm range was found near grain boundaries, and the impurity concentration dropped far from the grain boundaries. Further characterization on the distribution of deep levels, which affects minority-carrier lifetime, will be needed.

References

[1] S. Fujii, Y. Fukawa, H. Takahashi, Y. Inomata, K. Okada, K. Fukui, K. Shirasawa, Production technology of large area multicrystalline silicon solar cells, Tech. Dig. PVSEC-11 (1999) 123–126.

[2] J. Zhao, A. Wang, P. Campbell, M.A. Green, A 19.8 efficient honeycomb multicrystalline silicon solar cell with improved light trapping, IEEE Trans. Electron Devices 46 (1999) 1978–1983.
[3] R.H. Kingston, Switching time in junction diodes and junction transistors, Proc. IRE 42 (1954) 829–834.
[4] Y. Hayamizu, T. Hamaguchi, S. Ushio, T. Abe, F. Shimura, Temperature dependence of minority-carrier lifetime in iron-diffused p-type silicon wafers, J. Appl. Phys. 69 (1991) 3077–3081.